
Article:
Ramírez-González, J. orcid.org/0000-0002-6950-1255, Sinclair, D.C. orcid.org/0000-0002-8031-7678 and West, A.R. orcid.org/0000-0002-5492-2102 (2023) Impedance and dielectric spectroscopy of functional materials: a critical evaluation of the two techniques. Journal of The Electrochemical Society, 170 (11). 116504. ISSN 0013-4651

https://doi.org/10.1149/1945-7111/ad09fa

OPEN ACCESS

Impedance and Dielectric Spectroscopy of Functional Materials: A Critical Evaluation of the Two Techniques

To cite this article: Julia Ramírez-González *et al* 2023 *J. Electrochem. Soc.* **170** 116504

Journal of The Electrochemical Society, 2023 **170** 116504

Impedance and Dielectric Spectroscopy of Functional Materials: A Critical Evaluation of the Two Techniques

Julia Ramírez-González,[a] Derek C. Sinclair, and Anthony R. West[*,z]

Department of Materials Science and Engineering, The University of Sheffield, United Kingdom

Impedance and dielectric spectroscopies are closely related techniques for measuring the electrical properties of materials. The techniques differ in two ways. First, impedance measurements are usually made over several decades of frequency (i.e. broadband) whereas most dielectric measurements are made at fixed frequency. Second, time constants that control semicircles in impedance complex plane plots and peaks in permittivity or tan δ spectroscopic plots are not the same. Differences between the techniques are confined to data analysis procedures and interpretation since they use similar instrumentation for measurements and data collection. In impedance data, time constants represent conducting components and parallel resistance-capacitance (RC) combinations; in permittivity data, they represent dielectric processes and series RC combinations. Using broadband data, it is possible to (i) determine the best equivalent circuit to fit experimental data, (ii) unambiguously evaluate and assign resistance, capacitance, and time constant parameters to regions of the material being measured and (iii) quantify departures from ideality using constant phase elements, CPEs. Using fixed frequency, variable temperature data in either impedance or dielectric methodologies, it is possible to detect the presence of different electrical components that contribute to a data set. However, it is not possible to separate the effects of frequency and temperature in terms of equivalent circuits, nor to deconvolute, parametrise, quantify, and assign the results to different regions of the sample. The advantages of using broadband measurements are highlighted with two examples: calcium copper titanate, CCTO which is often, erroneously, described as a giant or colossal dielectric; lead magnesium niobate, PMN, the classic relaxor ferroelectric whose characteristic properties are controlled entirely by the presence of non-ideality, represented by a CPE, in its equivalent circuit.

 [DOI: 10.1149/1945-7111/ad09fa]

Manuscript submitted July 22, 2023; revised manuscript received October 31, 2023. Published December 6, 2023.

Impedance spectroscopy (IS) and dielectric spectroscopy (DS) are two techniques that are widely used for materials characterisation and electrical property measurement.[1–3] Each has its own identifiable research community, terminology and measurable materials parameters. They use similar instrumentation and there is often cross-over in which method to use for a particular material or problem. Nevertheless, the relationship between the two techniques is not clear. Although there are many similarities in data collection procedures, there are fundamental differences, especially in data analysis. This can lead to different, and often contradictory, viewpoints of electrical properties, especially whether the spectroscopic features that are measured refer to conducting or dielectric processes.

The essential features of each can be summarised as follows. IS uses variable frequency (broadband) data sets collected at fixed temperature. Data are analysed in terms of equivalent circuits made of resistance (R), capacitance (C) and sometimes, inductance (L) components of materials whose properties range from insulating to semiconducting. IS is particularly useful for materials that are inhomogeneous. Each electrically different region of a sample has a time constant consisting, ideally, of frequency-independent R and C parameters that are assumed to be connected in parallel. The different regions and their associated parallel RC elements are usually connected in series to give more complex equivalent circuits that represent the complete impedance response. Data on the component R, C parameters are separated and measured in the frequency domain using IS and the objectives are to (i) determine the most appropriate equivalent circuit, (ii) extract values of the component R, C parameters from the circuit equations and (iii) relate these parameters to characteristic features of the sample. In many cases, the parameters are not ideal but show frequency dependence which is taken into account in the circuit analysis.

The term Electrochemical Impedance Spectroscopy (EIS)[4] uses the same measurement and analysis procedures as IS but EIS usually focuses on low frequency, diffusion-related electrochemical reactions, whereas IS is used mainly for materials characterisation at higher frequencies, that also extend to lower frequencies for the study of sample-electrode impedances. In practice, there is no real difference between IS and EIS.

Dielectric spectroscopy, by contrast, traditionally uses fixed frequency, variable temperature, sweeps of permittivity and dielectric loss or tan δ to determine the time constants of dielectric relaxation processes. It is not possible to identify the most appropriate equivalent circuit from fixed frequency DS data, but nevertheless, the temperature dependence of dielectric processes, including activation energies, can be evaluated by combining a number of fixed frequency data sets.

Both IS and DS measure the time constants of electrically active components but for a particular material, ***they are not usually the same time constants***. IS time constants are commonly based on parallel RC circuit elements, each of which represents a conducting component, such as a bulk or grain boundary region. DS time constants obtained from peaks in dielectric loss and tan δ data are, by contrast, based implicitly on either series RC combinations or more complex circuits involving both series and parallel RC combinations and usually represent localised conductivity or relaxation such as dipole reorientation. One great advantage of using an equivalent circuit-based data analysis methodology for either IS or broadband DS is that all possible time constants can be identified and measured in principle. Since IS and DS use the same, or parts of the same, data sets, there should be no fundamental difference in results obtained from IS and DS once it is recognised that they may highlight different features of data sets and different time constants.

The electrical properties of homogeneous materials such as most single crystals, glasses and many ceramics correspond to those of single phase, bulk components. Heterogeneous materials have at least two components whose properties differ and the overall properties may be dominated by one component alone or a combination of components. IS has been exceptionally useful for characterising both homogeneous and heterogeneous materials

*Electrochemical Society Member.
[a]Present address: Department of Materials, University of Oxford, Oxford, United Kingdom.
[z]E-mail: a.r.west@sheffield.ac.uk

because it can determine their ***electrical microstructure*** which may, or may not, be the same as the microstructure seen using electron microscopy techniques. By contrast, fixed frequency DS is usually used for homogeneous, insulating materials that have components associated with local *ac* losses. Leakage conductivity through an insulating bulk may also be present in DS data and is a source of temperature-dependent background loss.

The time constant, τ, of an element is given by the magnitude of its RC product, either series or parallel, i.e.

$$\tau = \mathrm{RC} \quad [1]$$

and this controls the frequency at which it can be observed and measured in impedance and dielectric spectra. The frequencies of peak maxima, $\omega_{max} = 2\pi f_{max}$ are related to the time constant, ideally, by:

$$\omega_{max}\mathrm{RC} = 1 \quad [2]$$

Resistances, and therefore the time constants, of thermally-activated processes are temperature-dependent and both IS and DS benefit greatly from measurements over a range of temperatures. Capacitances usually have little temperature-dependence unless the materials are (incipient) ferroelectric, but the magnitudes of the capacitances depend on geometric factors and are very useful in distinguishing between bulk and interfacial phenomena.

From IS studies on many materials, it is apparent that R and C parameters are rarely ideal but show frequency-dependence. This has major implications for data analysis methodologies. In earlier times, empirical distribution of relaxation time (DRT) functions were used to fit frequency-dependent conductivity and dielectric data.[5,6] More recently, constant phase elements (CPEs), based on Jonscher's Law of Universal Dielectric Response (UDR),[7] are often found to represent accurately departures from ideality over wide frequency ranges and are added to equivalent circuits to allow quantitative fitting and analysis of impedance data.[8] CPEs must also contribute to fixed frequency DS datasets and be a source of non-ideality in DS peak shapes which traditionally, are fitted using empirical DRT functions. However, it is not possible to characterise fully the CPEs using fixed frequency, variable temperature data sets.

The development of IS began with the availability of commercial instrumentation to measure electrical property data over wide frequency ranges and the proposed use of complex plane analysis by Bauerle[9] to separate and characterise the electrical properties of heterogeneous, conducting ceramics. IS is a standard method applicable to a variety of materials and systems. Isothermal data are collected over a wide frequency range, routinely from mHz to MHz. Grain (or bulk), grain boundary and electrode-sample contact effects are usually regarded as series-connected and equivalent circuits are used, directly or implicitly, to extract resistance and capacitance values of the different electrically-active components or regions of a sample.[10] However, there are still no universally-accepted strategies to identify ab initio the most appropriate equivalent circuit for the analysis of IS data, especially for real systems in which the R and C components show non-ideal frequency dependence. This is due partly to the difficulty in distinguishing between i) non-ideality that is an intrinsic property of homogeneous regions of a sample and ii) overlapping impedances associated with sample heterogeneity. It is also partly because of the truism that, for a given data set, it is always possible to find more than one equivalent circuit to fit the data. The key question that is always present, but often not answered fully is, therefore: which circuit best represents the material or system being measured?

DS takes historical precedence over IS and has been used widely for many years to study relaxation processes in polymeric and glassy materials.[11–13] The focus of data analysis has been to identify time constants from peak maxima, either from variable frequency sweeps at fixed temperature (similar to IS) or variable temperature sweeps at fixed frequency, although in the early years of DS only the second of these was a realistic possibility. Data are usually presented as permittivity and tan δ or dielectric loss parameters which lead to the characterisation of different relaxation processes over different temperature ranges.[14–17] Most dielectric materials also show residual or leaky *dc* conductivity, especially at higher temperatures and this appears as background dielectric loss on which the various dielectric processes are superposed.

The basic principles of IS, DS techniques and data analysis methodologies are well-established and are not covered in detail here; use of IS to characterise electroceramic materials is covered in an earlier review.[10] Various instruments that collectively, cover a very wide range of measuring frequencies are available on the market and also, are not discussed here. Instead, we focus on data analysis methodologies, equivalent circuits, comparison of IS and DS techniques and the inclusion of DRTs and CPEs in the interpretation of non-ideal impedance data.

Experimental Considerations and Data Collection

IS and DS are based on the same basic principle of measuring the resistance and reactance of a material or system subjected to a variable frequency, small signal *ac* voltage or current. The applied signal is of known amplitude (V_0 or I_0) and frequency (expressed as f, Hz or $\omega = 2\pi f$, rad/s). The responding signal has the same frequency but is phase-shifted by ϕ according to the capacitive and inductive characteristics of the system. The voltage to current ratio gives the magnitude of the impedance:

$$|Z| = \frac{V_0}{I_0} \quad [3]$$

The impedance is a complex function and can be expressed in three forms: polar, exponential or rectangular, using Euler's identity:

$$Z^* = |Z|\angle\varphi = |Z|\ e^{j\varphi} = |Z|(\cos\varphi + j\sin\varphi) = Z' + jZ'' \quad [4]$$

In fixed frequency DS measurements, LCR meters are commonly used to take dielectric measurements at regular time intervals, e.g. every 60 s, and synchronised with a furnace that provides a constant heating rate. For IS measurements, impedance analysers perform frequency sweeps at a fixed temperature that, depending on the instrumentation, could routinely be between 10^{-3} and 10^{7} Hz. This wide frequency range may, nevertheless, be insufficient to cover the full range of time constants of the impedance components and it is common practice to perform measurements at different temperatures both to access a more complete range of time constants and to determine the temperature dependence of component R, C parameters.

The IS and DS techniques make use of the frequency domain. Time domain measurements can also determine relaxation processes and in principle, could cover a complete range of frequencies. All that is required is to record the excitation and recovery time of the perturbation.[1] For example, the galvanostatic pulse technique,[18] uses a rectangular pulse to pass a current through the sample and the resulting potential difference is measured. If necessary, time-to-frequency Fourier transformation techniques can be applied to translate results to the frequency domain.[1] Time domain measurements are not widely used to characterise functional materials, however and are not considered further here.

In order to obtain accurate R and C values from IS or DS data, it is necessary to eliminate, or correct, stray instrument or sample holder interferences. This is particularly the case if accurate bulk capacitance data in the picoFarad range are to be measured since sample holders or "jigs" may have intrinsic capacitances in the pico- to nano-Farad range. Frequency-dependent data on open circuit, without the presence of a sample, may be recorded to obtain the parallel, or "blank" capacitance of the measuring system and can be subtracted from data recorded with a sample in place to give the sample capacitance. In cases where the sample resistance is small, the inductance of the electrode wires, connections and instrumentation may be substantial and may be

corrected, together with lead resistances, by subtracting data obtained from measurements on closed circuit.

The sample dimensions need to be considered since R and C values are geometry-dependent whereas the associated resistivity (ρ) and permittivity (ε) are fundamental, geometry-independent parameters, as follows:

$$\text{Cell constant (g)} = \frac{\text{sample thickness (d)}}{\text{electrode area (A)}} \quad [5]$$

$$\rho = \text{R/g} = \text{R}\,\frac{\text{A}}{\text{d}};\ \text{typical units } \Omega\text{cm} \quad [6]$$

$$\varepsilon = \text{C g} = \text{C}\frac{\text{d}}{\text{A}};\ \text{units Fcm}^{-1} \quad [7]$$

$$\varepsilon' = \varepsilon/\varepsilon_0 = \text{C/C}_0;\ \text{no units} \quad [8]$$

where ε is the (absolute) permittivity, ε' is the relative permittivity or dielectric constant of a material relative to that of free space, $\varepsilon_0 = 8.854 \times 10^{-14}$ Fcm^{-1} and C_0 is the vacuum capacitance of the measuring cell without a sample. It is straightforward to correct data for the overall geometry of a sample but less easy to determine the geometries of individual components such as grain boundaries. Sometimes, this is attempted but in other cases, data are corrected only for the overall geometry.

In addition to the parameters and terminology for ε and ε', sometimes the term effective permittivity, ε_{eff} is used. It is the same as ε' in Eq. 8 in which the capacitance is simply the capacitance at a specific, measured frequency. ε_{eff} may be frequency-dependent for two reasons. Either the permittivity of a single phase, homogeneous material may show intrinsic frequency dependence due to non-ideality in the associated equivalent circuit. Or there may be an overlap in permittivity data from two different regions of a sample.

The intrinsic permittivity of many bulk materials is frequency-dependent and decreases gradually to a constant value at high frequencies, where it is given the symbol ε_∞ with associated capacitance C_∞. ε_∞ may be regarded as the limiting, high frequency value of an intrinsic material property, in the same way that the zero frequency resistivity of a single phase, homogeneous sample, ρ_{DC}, is a limiting low frequency value free from higher frequency *ac* conductivities. Advantages of equivalent circuit analysis of broad-band data are that it provides a methodology to deconvolute different contributions to the overall impedance or dielectric response and to separate the effects of non-ideality and sample heterogeneity; neither of these are possible using fixed frequency data.

Much of the continuing literature concerning "giant permittivities" and "colossal permittivities" has arisen from the measurement of thin layer effects that are not corrected for their geometries and instead, are often misinterpreted as bulk phenomena.[19–21] This confusion has also obscured the study, and understanding, of possible novel high permittivity intrinsic bulk phenomena[22,23] although this is still a topic of active discussion.[24,25]

The time constant, τ of an RC element is dimensionless since:

$$\tau = \text{RC} = \rho\varepsilon \quad [9]$$

This is critically important for the study of ceramic materials since, ideally, a single time constant should apply to all grains of a homogeneous sample. Whereas R and C are geometry-dependent parameters, their geometries cancel in the RC product. Consequently, if the grains (and grain boundaries) consist of the same material, structurally and electrically, in a fully dense homogeneous ceramic whose properties are isotropic, then a single time constant should be applicable, independent of grain size and orientation. Effectively, the time constant of a multigrain ceramic would be the same as that of a single crystal of the same composition.

In many cases, grain boundaries are electrically-distinct from grains, have different time constants and should therefore appear as separate impedances. Two kinds of grain boundary impedance may be identified. If grain boundaries are different from grains in terms of their structure, composition or dopant distribution, their temperature-dependent conductivities are likely to have different activation energy from that of the grains and can be readily recognised from their temperature-dependent conductivity Arrhenius plots.[10] Alternatively, the grain boundaries may have the same composition as the grains but form a neck or constriction between grains in a ceramic that is porous or only partially densified. The necks are responsible for the grain boundary resistance which, therefore, has similar activation energy to that of the grains, but the grain boundary capacitance is modified by the presence of insulating air gaps, giving rise to a different time constant and a separate impedance RC element.[26] A strong indication of the nature of a grain boundary impedance, therefore, is whether its activation energy is similar to, or different from, that of the grains.

Fundamentals of Data Analysis: Parallel and Series RC Elements, Equivalent Circuits, Impedance Formalisms and Data Presentation Formats

The usual starting point in representing the electrical properties of an ideal, single phase, non-ferroelectric homogeneous material is the ***parallel RC element***, Fig. 1a; R represents the *dc* resistance and C is the bulk capacitance which is often the limiting high frequency capacitance, C_∞, free from lower frequency polarisation processes. If the material has infinitely large resistance, the element reduces to a capacitor C, (b), for which the permittivity of the dielectric material [measured between the plates of a capacitor] is given by Eq. 7. In dielectric terminology, Fig. 1a is also the starting point to represent a ***leaky dielectric*** since the value of R is no longer infinite and is in parallel with C.

For heterogeneous conducting materials, each impedance component, such as the sample bulk, R_b, C_b and grain boundary, R_{gb}, C_{gb}, can be represented ideally by (a) and these elements are connected in series in (c) for the usual situation in which $R_{gb} > R_b$. An additional parallel RC element, $R_{ct}C_{dl}$ may represent the sample-electrode contact impedance, especially for materials that are ionically-conducting and attached to blocking electrodes (d); R_{ct} represents the charge transfer resistance and C_{dl} represents the double layer blocking capacitance. In reality, parallel RC elements are rarely ideal because the R and C components exhibit frequency dependence over all or part of the measuring frequency range. This is usually represented by adding a CPE in parallel with R and C, as shown for one element in (e).

There are four commonly-used complex formalisms for presenting impedance data and their inter-relationships:

$$\text{Impedance, } Z^*$$

$$\text{Admittance, } Y^* = [Z^*]^{-1} \quad [10]$$

$$\text{Electric modulus, } M^* = j\omega C_0 Z^* \quad [11]$$

$$\text{Permittivity, } \varepsilon^* = [M^*]^{-1} = [j\omega C_0 Z^*]^{-1} = [j\omega C_0]^{-1} Y^* \quad [12]$$

For the circuit shown in Fig. 1a, the R and C elements are in parallel and therefore, the first step is to write circuit equations in terms of admittances since admittances add in parallel:

$$Y^* = Y' + jY'' = \frac{1}{\text{R}} + j\omega\text{C} \quad [13]$$

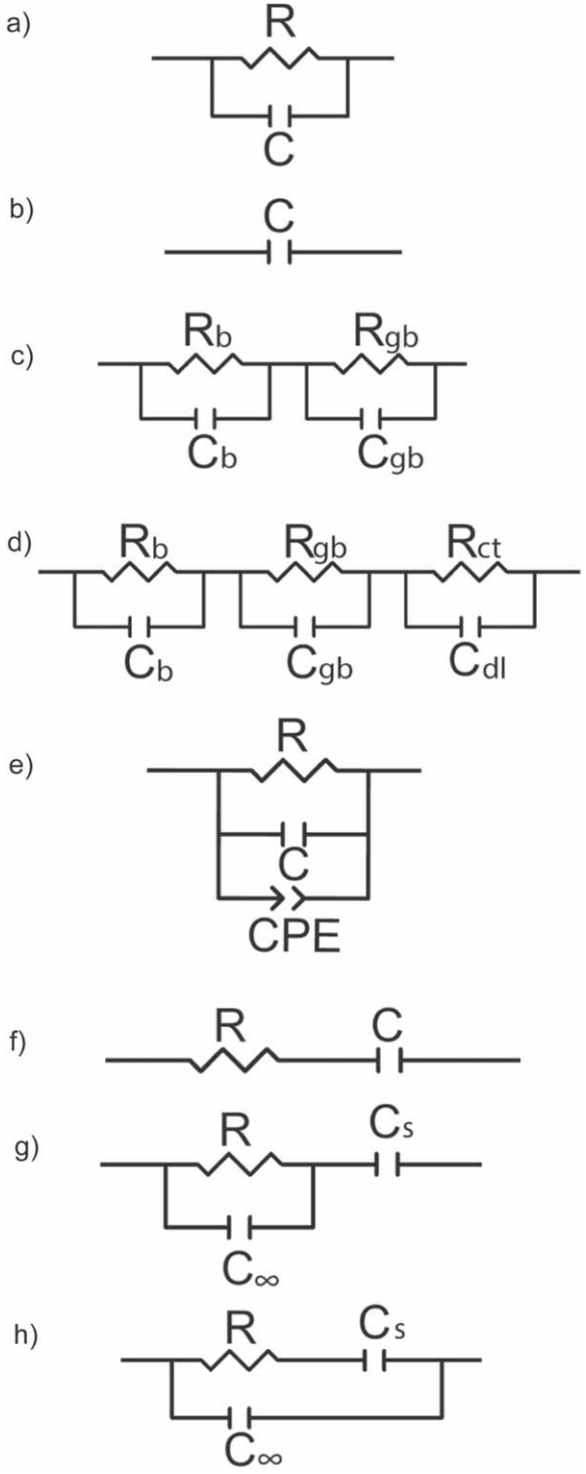

Figure 1. Equivalent circuits consisting of various R, C combinations in parallel and/or in series.

and the equation separates simply into real, Y′ and imaginary, Y″ components. Presentation of data for this circuit in the ε^* formalism is also simple since:

$$\varepsilon^* = \varepsilon' - j\varepsilon'' = [j\omega C_0]^{-1}Y^* = CC_0^{-1} + [j\omega C_0 R]^{-1} \quad [14]$$

In the impedance and electric modulus formalisms, separation of the real and imaginary components is less straightforward, Eqs. 15, 16:

$$Z^* = Z' + jZ'' = (Y^*)^{-1}$$

$$= \frac{R}{1 + (\omega RC)^2} - jR\left[\frac{\omega RC}{1 + (\omega RC)^2}\right] \quad [15]$$

$$M^* = M' + jM'' = \frac{C_0}{C}\left[\frac{(\omega RC)^2}{1 + (\omega RC)^2}\right]$$

$$+ j\frac{C_0}{C}\left[\frac{\omega RC}{1 + (\omega RC)^2}\right] \quad [16]$$

The data are presented most commonly in two ways, either in their complex planes (also known as Nyquist plots) on linear scales, giving rise to semicircles in Z^* and M^*, Figs. 2a, 2b or as spectroscopic plots (also known as Bode plots) on linear-log scales, giving rise to Debye peaks of Z″, M″ vs log frequency (c, d). Complex plane presentations of Y^* and ε^* are shown in (e, f) and are very simple for this circuit.

A third presentation format, especially in DS studies, is as tan delta, defined as $\varepsilon''/\varepsilon''$ and for a parallel RC element given by:

$$\tan\delta = \varepsilon''/\varepsilon' = 1/\omega RC \quad [17]$$

tan δ decreases exponentially with increasing frequency, or linearly on logarithmic scales, as shown in (g).

The starting point in the DS methodology of data analysis is the series RC element, Fig. 1f. This is a dielectric circuit since it has no finite resistance in parallel with the capacitance. But, it does have a series resistance which may represent a local charge displacement process that gives short range, *ac* conductivity. Since R and C are in series, the first step in writing circuit equations is as series-connected Z^* and M^* which give very simple complex plane plots, Figs. 3a, 3b. Converting the equations to ε^* and Y^* formalisms gives rise to Debye peaks in spectroscopic ε'', Y″ plots and semicircles in the associated complex planes, Eqs. 18, 19, and Figs. 3c–3f; tan δ, Eq. 20 increases exponentially with frequency, (h).

$$\varepsilon^* = \varepsilon' - \quad j\varepsilon'' = \frac{C}{1 + (\omega RC)^2} - jC\left[\frac{\omega RC}{1 + (\omega RC)^2}\right] \quad [18]$$

$$Y^* = Y' + jY'' = \frac{1}{R}\left[\frac{(\omega RC)^2}{1 + (\omega RC)^2}\right] + j\frac{1}{R}\left[\frac{\omega RC}{1 + (\omega RC)^2}\right] \quad [19]$$

$$\tan\delta = \omega RC \quad [20]$$

Consideration of Figs. 2, 3 which are based on parallel and series RC elements and their associated equations, illustrates the fundamental distinction between IS and DS methodologies as they are applied, respectively, to conducting or dielectric features of materials. Thus, complex plane semicircles and spectroscopic Debye peaks occur with parallel RC combinations in Z^*, M^* but with series RC combinations in ε^*, Y^*. More complex equivalent circuits of real materials usually have combinations of series and parallel RC elements; any of the four formalisms given in Eqs. 10–12 can be used for data analysis, bearing in mind that the spectroscopic peaks, complex plane semicircles and associated time constants may differ.

We next consider the most appropriate circuit to represent DS data for dielectric relaxation processes, such as dipolar reorientation, that do not contribute to *dc* conductivity. Circuits f, g and h are the main possibilities in principle since they all have a blocking capacitance C_s. For most dielectrics, their limiting high frequency permittivity, ε_∞ is small with typical values in the range 5–10. Consequently, C_∞ is small and therefore, $C_\infty \ll C_s$. With this assumption, simulations using circuits (g) and (h) are almost identical, as shown for Z^* and ε^* in Fig. 4; values

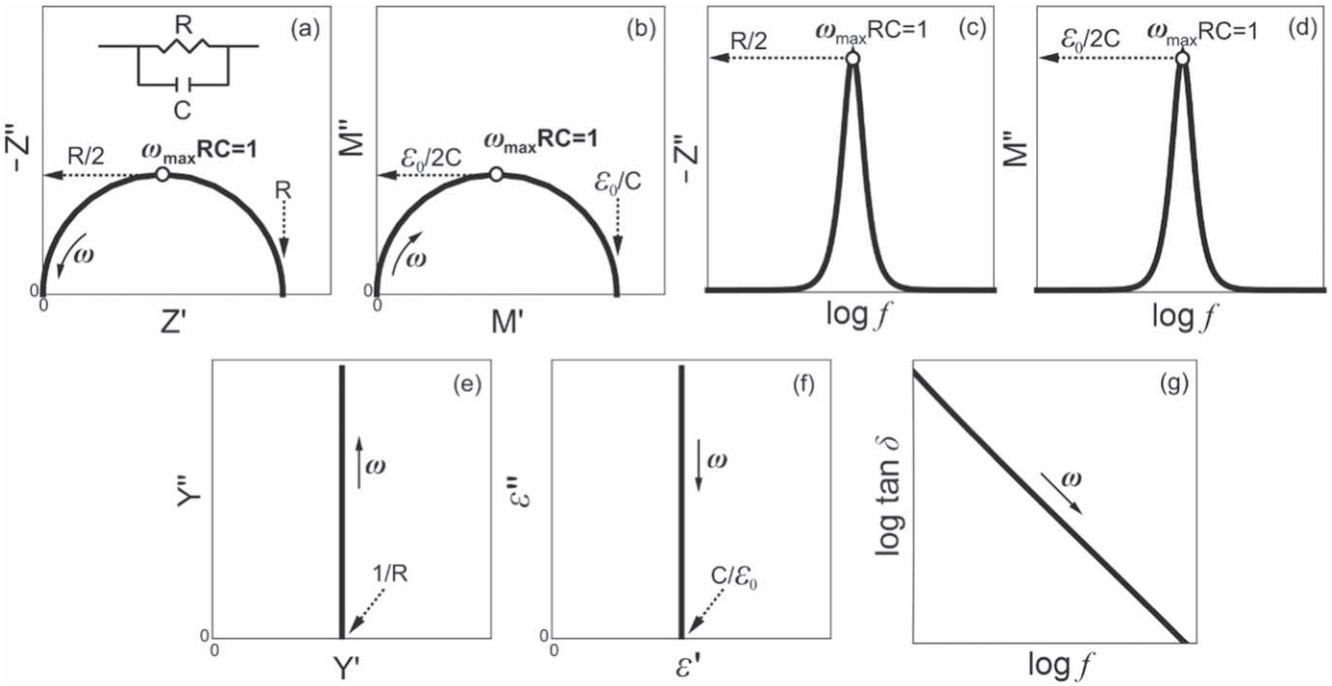

Figure 2. Circuit simulations for a parallel RC element.

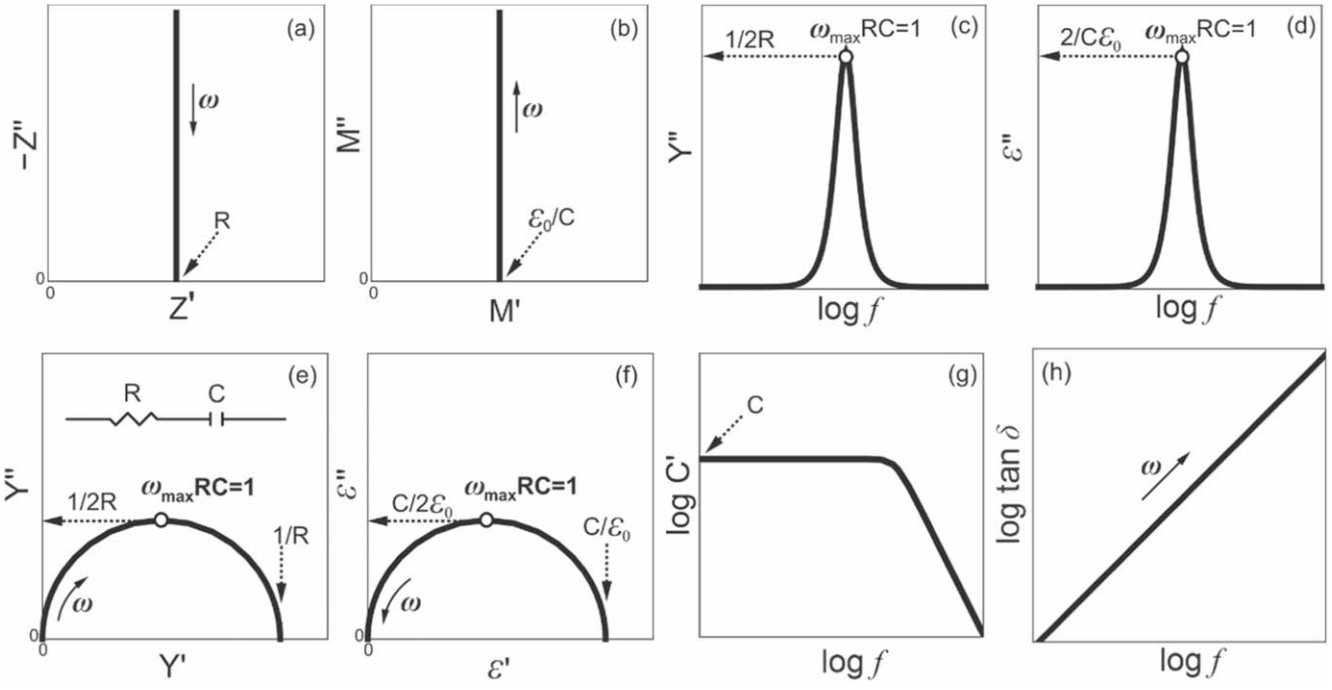

Figure 3. Circuit simulations for a series RC element.

of the intercepts are given in Table I. Both circuits give a low frequency spike in Z* (a) controlled by C_s and a high frequency semicircle that does not pass through the origin in ε* (b, inset). Spectroscopic plots of C′ show low and high frequency plateaux (c) for both circuits [note: C′ represents the capacitance obtained from impedance data and is equal to the real part, ε', of the complex permittivity, ε*; the parameters C' and ε' are used interchangeably, here and elsewhere, to label the same parameter]. tan δ shows a change of slope from 1 to −1 in logarithmic plots against frequency, (d) since at low frequencies, the RC_s series component and time constant dominates ε' whereas at high frequencies, the RC_∞ parallel component dominates ε'.

All circuits (f-h) give similar low frequency behaviour therefore but at higher frequencies, capacitance C_∞ features strongly for g,h but not for f, as seen by (i) comparing Figs. 3h and 4d for tan δ and (ii) comparing Figs. 4c and 3g for C′ or ε'. Care is needed in analysing dielectric data in terms of equivalent circuits and in particular, whether experimental data extend to frequencies that are high enough to require the inclusion of C_∞.

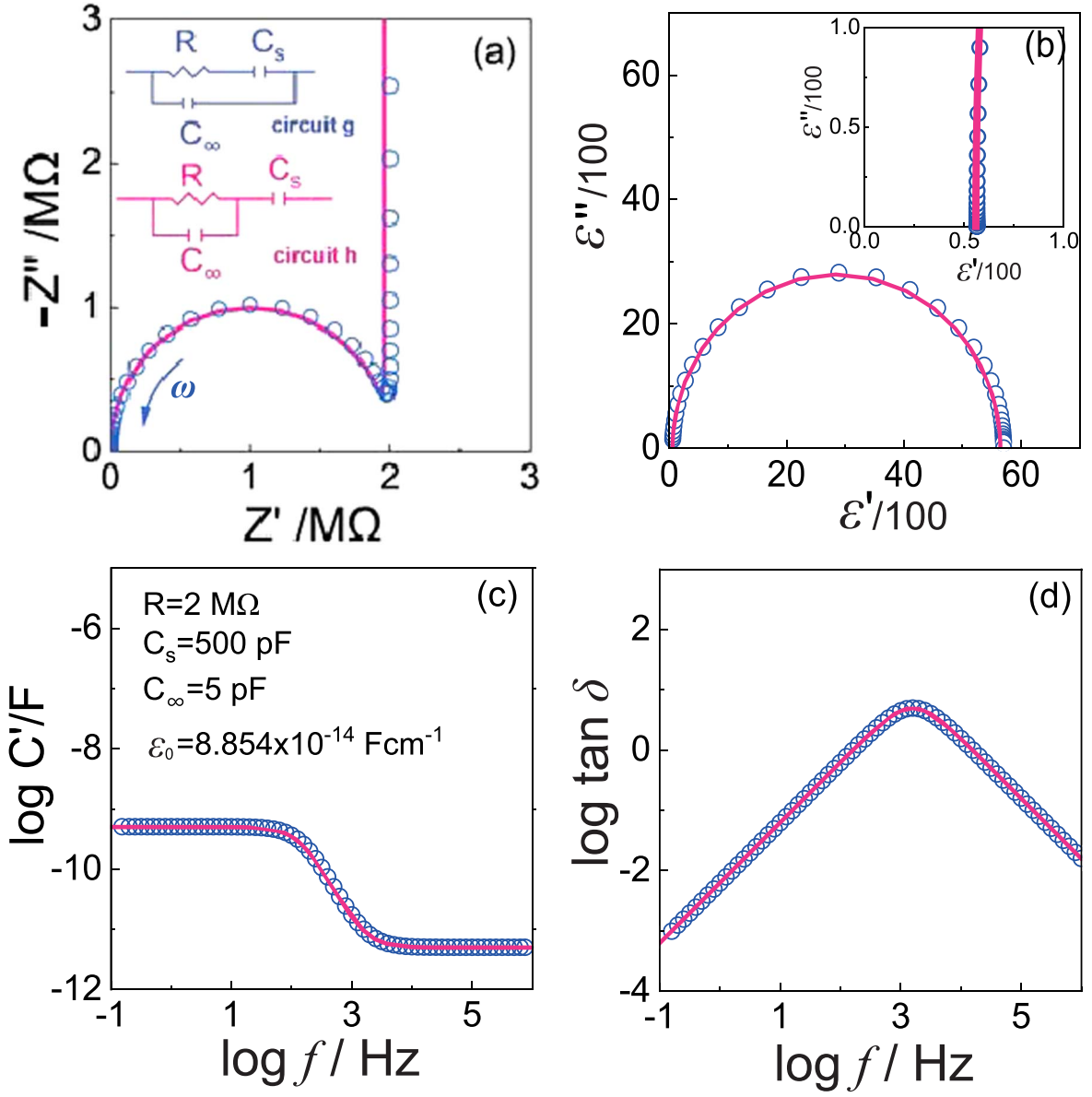

Figure 4. Two possible circuits to represent dielectric relaxation and associated simulations based on parameter values given in Table I.

The potential difficulties that can arise in understanding the origin of time constants and their link to equivalent circuits may be illustrated for the case of a ceramic that has electrically active bulk and grain boundary impedances. These are represented by a series combination of parallel RC elements (provided the grain boundaries are more resistive than the grains), Figs. 1c, 1d. The time constant of each controls the presentation of IS data using the impedance formalism and for instance, each parallel RC element gives rise to a semicircle (ideally) in impedance complex plane plots. By contrast, DS methodology focuses on the time constant of series RC combinations such as that for a grain boundary resistance of one parallel RC element in series with a capacitance of another RC element and gives rise to a semicircle in permittivity complex plane plots. A spectroscopic plot of tan δ against frequency may therefore contain a peak that represents this series RC combination. In using the IS and DS techniques, it is clearly vital in analysing the data to know which R, C components contribute to a particular peak or semicircle and its associated time constant.

Two other terminologies that are sometimes used to describe specific methods of data presentation are admittance spectroscopy and impedance and modulus spectroscopy. Admittance spectroscopy is similar to dielectric spectroscopy, although the emphasis is on conductive processes that occur in parallel with each other.[27–30] Impedance and modulus spectroscopy involves combined plots of Z″ and M″ against frequency since Z″ highlights the most resistive components of a sample whereas M″ highlights the component with the smallest capacitance, which is usually the bulk; this can be useful in assigning the most appropriate equivalent circuit to a particular dataset.[31–34]

Table I. Low and high frequency intercepts of ε′ spectra for circuits g and h from Fig. 1.

	ε′ intercepts	
	Low frequency	High frequency
Circuit g	$C_s + C_\infty$	C_∞
Circuit h	C_s	$(C_sC_\infty)/(C_s + C_\infty)$
if $C_\infty \ll C_s$		
Circuit g	$\sim C_s$	C_∞
Circuit h	C_s	$\sim C_\infty$

Departures from Ideality, DRTs and Inclusion of CPEs in Equivalent Circuits

Distribution of relaxation times, DRT.—An early indication that departures from ideality may be an intrinsic feature of homogeneous conducting materials was the widespread observation of high frequency dielectric losses or conduction losses in ionically conducting alkali silicate and borate glasses. Such materials are usually single phase and do not have grain boundaries or other interfacial effects which may complicate the impedance response. They typically showed a frequency-independent conductivity or conductivity plateau, Y' at low frequencies that represented long range *dc* conduction, followed by an increased conductivity at higher frequencies that represented short range or localised, *ac* conductivity. Such high frequency conductivity data were traditionally fitted to DRT functions and models were developed that often involved a distribution of barrier heights for ion hopping within an amorphous glass network.[35]

Several DRT functions - Cole-Cole,[5] Cole-Davidson,[36] and Havriliak-Negami[37] - were employed to fit departures from ideality at high frequencies, especially in DS methodologies. In these, the parameters α and β represent non-ideality in the complex permittivity, $\varepsilon(\omega)^*$ of dielectric relaxation processes:

$$\varepsilon^*_{(\omega)} = \varepsilon_\infty + \frac{\varepsilon_s - \varepsilon_\infty}{[1 + (j\omega\tau)^{(1-\alpha)}]^\beta} \quad [21]$$

For the ideal case that $\alpha = 0$ and $\beta = 1$, Eq. 21 reduces to 22 which represents the equivalent circuit shown in Fig. 1g:

$$\varepsilon^*_{(\omega)} = \varepsilon_\infty + \frac{\varepsilon_s - \varepsilon_\infty}{1 + j\omega\tau} \quad [22]$$

This circuit is essentially the dielectric circuit (f) to which has been added the capacitance that represents the limiting high frequency permittivity of the material (C_∞). It is not clear whether any quantitative information concerning, for instance, conduction mechanisms for ion hopping, could be obtained from fits to Eq. 21 and the values of α and β. However, as the quality and extent of variable frequency IS and DS data has increased with improvements to measuring instrumentation, the DRTs were often found to fit experimental data over only limited frequency ranges. In addition, the validity of the DRT concept to represent departures from ideality in IS and DS data was called into question by Jonscher's discovery of the power law nature of the frequency-dependent dispersion in conductivity or susceptibility of widely-different materials, now known as the Universal Law of Dielectric Response, UDR.[7,38–40] The origin of DRTs in ionically-conducting materials such as alkali silicate glasses had been attributed to a distribution of barrier heights for an alkali metal ion hopping through an amorphous network, but it became difficult to reconcile this with a model based on UDR that involves a power law distribution of physical barrier heights. DRTs are still used to fit non-ideality in various cases but essentially, these are empirical fits that are not based on a physical model of the processes responsible.

Constant phase element, CPE.—There is now increasing acceptance that power law behaviour, represented by constant phase elements, can usefully and quantitatively represent non-ideal behaviour over wide frequency ranges for many single phase, homogeneous materials. Similar power law behaviour in the high frequency ionic conductivity of single crystal Na beta-alumina[41] showed that this was not exclusively a property of the amorphous state. As well as their use in the fitting and analysis of bulk ionic conductivity data, CPEs are widely used in the characterisation of electrochemical processes at lower frequencies which are associated with sample-electrode interfaces and diffusion impedances.[42–44]

There are several major advantages to the inclusion of CPEs in equivalent circuits. First, they acknowledge the ubiquitous presence of non-ideality in impedance data sets of homogeneous, bulk materials. Second, their characterisation provides additional insight into bulk conduction mechanisms. Third, they allow accurate fitting of impedance data of heterogeneous materials to equivalent circuits, which enables a better understanding and quantification of the factors responsible for the heterogeneity.

The bulk response of many materials can be represented accurately by combination of R, C and CPE in parallel, Fig. 1e. A CPE is a parallel combination of a frequency-dependent resistor and capacitor and is an admittance of the form:

$$Y^* = A\omega^n + jB\omega^n \quad [23]$$

where $j = \sqrt{-1}$. A CPE gives a power law response of both conductivity and capacitance (permittivity or susceptibility) data over a wide frequency range. Circuit Fig. 1e gives a power law dispersion in conductivity, Y′ at high frequency that is characterised by the value of n where $0 < n < 1$, Fig. 5a. At lower frequencies, long range conductivity through bulk and/or grain boundary regions dominates the data and the contribution of the CPE to Y′ is minimal. However, the capacitive component of the CPE becomes increasingly important with decreasing frequency and may be seen as a dispersion of value $(n-1)$ in capacitance, C′, Fig. 5b. Very many examples of such power law behaviour in a wide range of materials have been reported and their recognition led to the proposal and naming of the UDR Law by Jonscher.[3,7,38–40]

A CPE reduces to a simple resistor when $n = 0$ and to a capacitor when $n = 1$. Almond, Vainas and Bowen[45–49] resolved the question of the significance of n with intermediate values. They showed that an equivalent circuit consisting of a network of many series and parallel RC connections, in which the magnitudes of R and C are kept constant, gives a power law-dependent conductivity in which n is given by the ratio of series to parallel connections in the circuit. Prior to this, the significance of n was not known although its recognition and measurement clearly had value in providing a way to fit and describe experimental data successfully.

It has been found that the bulk properties of many conducting materials may be represented best by the addition of a CPE in parallel with R and C, Fig. 1e. The admittance of this circuit is:

$$\begin{aligned} Y^* &= 1/R + j\omega C + A\omega^n + jB\omega^n \\ &= (1/R + A\omega^n) + j(\omega C + B\omega^n) \end{aligned} \quad [24]$$

where B and A are inter-related by:

$$B/A = \tan(n\pi/2) \quad [25]$$

The presence of the CPE modifies the responses of all four formalisms from the ideal given by Eqs. 10–12 and the changes depend on the magnitudes of n and A. We do not document here all the variations that may be seen, but note some key points associated with the most commonly-used methods of data presentation as follows:

(i) In the impedance complex plane, the ideal semicircular shape for a parallel RC element, becomes depressed and may become asymmetric; the low frequency intercept corresponds to resistance R and is not influenced by the CPE.

(ii) The log Y' spectroscopic plot, Fig. 5a is a simple addition of the *dc* conductivity, R^{-1} which dominates at low frequencies and the power law conductivity of the CPE with slope n that dominates at high frequencies. The cross-over between *dc* conductivity and power law is controlled by the value of A.

(iii) The log C′ spectroscopic plot, Fig. 5b is a simple addition of the power law capacitance of the CPE with slope $(n-1)$ at low frequencies and the bulk capacitance C at high frequencies. Similarly, the cross-over between the two regions is controlled by the value of B.

(iv) The M″/Z″ spectroscopic plots, Fig. 5c are not ideally Debye-like.[32] First, they are broadened on the low frequency

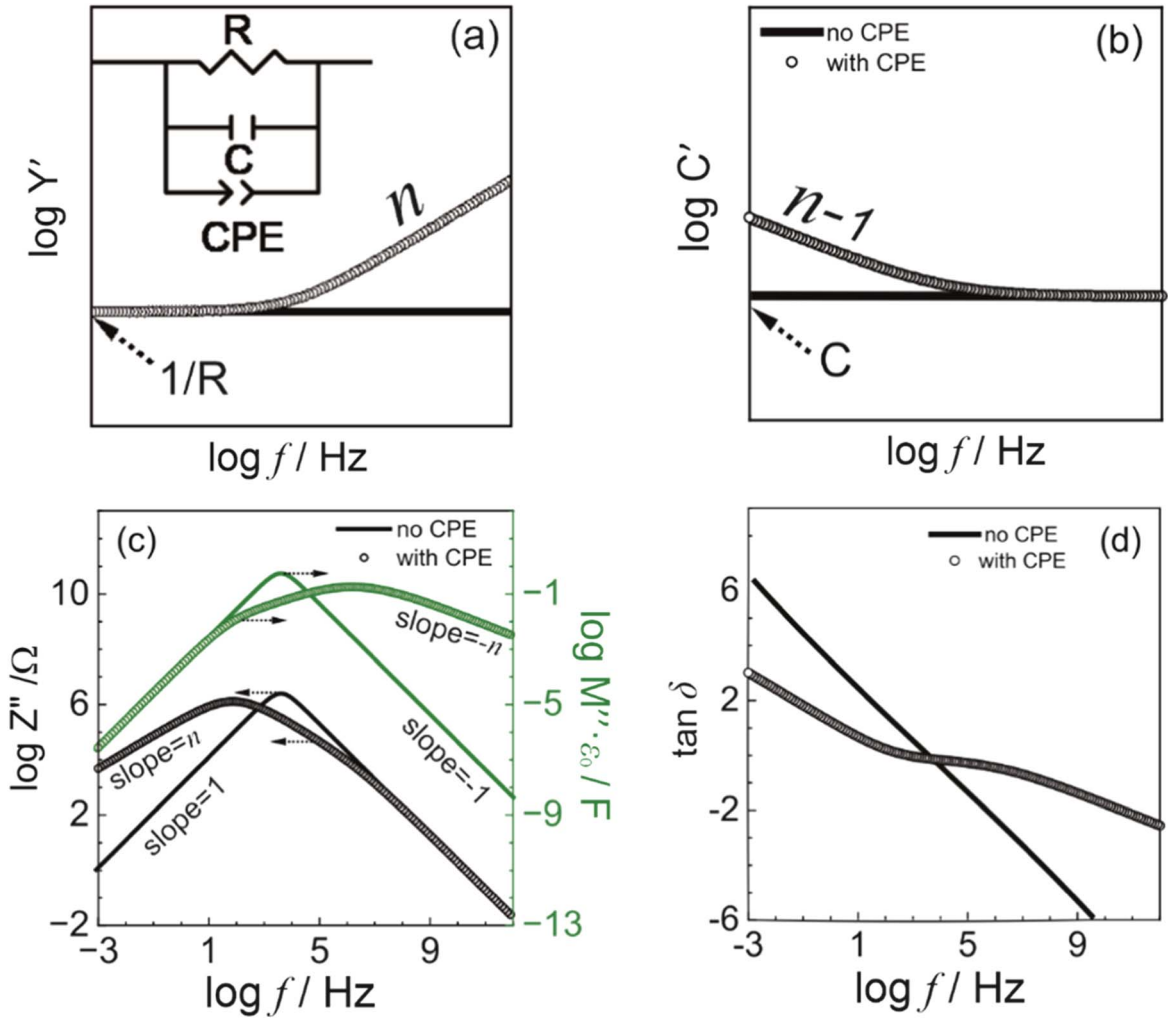

Figure 5. Simulations showing the effect of adding a CPE to a parallel RC element.

side for Z″ and on the high frequency side for M″. Using log-log scales to present M″/Z″ spectroscopic plots in (c), it is clear that a Debye peak has slopes of 1 and −1 on the low and high frequency sides, respectively, whereas the CPE n value controls the slopes which are n for Z″ at low frequency and $-n$ for M″ at high frequency. On the more commonly used linear-log scales, the non-ideality appears as a tail and asymmetric broadening on the low/high frequency side of the two peaks.

(v) The M″/Z″ peak maxima no longer obey the simple relation $\omega_{max}\tau = 1$, Eq. 2 but are displaced such that f_{max} for M″ is greater than f_{max} for Z″ (c). For a similar reason, the semicircle maximum in Z* does not correspond exactly to Eq. 1. It is important to note that the frequently-observed separation of M″/Z″ peak maxima in experimental data **may be** a consequence of non-ideality represented by the CPE but needs to be distinguished from possible peak separation associated with sample heterogeneity.

(vi) The tan δ spectroscopic plot for circuit Fig. 1a, which is linear on logarithmic scales, becomes very non-linear with inclusion of the CPE in the circuit for a parallel RC element, as shown in Fig. 5d. We do not give here an overview of the possible deviations of tan δ plots from ideality, either for this, or more complex circuits: it is difficult enough to rationalise the frequency dependence of separate ε' and ε'' plots without considering the frequency dependence of tan δ, i.e. the ε'': ε' ratio.

The grain boundary impedances of many materials are also usually modelled by circuit Fig. 1e and contain a CPE in parallel with R and C. It can be difficult to obtain grain boundary impedance data that are completely separate from bulk impedance data, but with good quality datasets, it is usually possible, and necessary, to add a CPE to model the grain boundary response as part of the overall impedance response. Difficulties arise generally with circuits that contain several contributing impedances, from bulk, grain boundary and electrode contacts and especially if two or three CPEs are added, since the CPEs are not single-valued but are frequency dependent. Care is therefore required in finding the most appropriate equivalent circuit for datasets with several contributing impedances; strategies for doing this have been proposed but are beyond the scope of this review.

We next give two examples which illustrate the distinction and correlation between broadband IS and fixed frequency DS techniques. Broadband data collection is linked to equivalent circuit analysis. We conclude that this leads to more comprehensive understanding of the origins of conductive and capacitive properties of functional materials than is possible using fixed frequency DS data alone.

Case study 1: Calcium Copper Titanate, CCTO and its "Giant" Permittivity

The electrical properties of the ceramic material $CaCu_3Ti_4O_{12}$ (CCTO) have generated much interest as they exhibit so-called giant or colossal permittivity.[19,21] In order to understand the origin of this

effect and distinguish between geometry-controlled high permittivities associated with thin regions of a sample and much lower intrinsic permittivities associated with the sample bulk, it was necessary to use broadband IS data. A combination of simulations and experimental data show that fixed frequency tan δ and permittivity data highlight a time constant that is associated with sample heterogeneity and in particular, the series combination of a small resistance associated with the ceramic bulk and a high capacitance associated with an interfacial region. Details are as follows.

CCTO is a member of a series of cubic perovskite-type compounds (space group *Im*−3) based on general formula $AA'_3Ti_4O_{12}$ where the corner sharing TiO_6 units are heavily tilted ($a^+a^+a^+$ in Glazer notation) and the Ca and Cu ions form a 1:3 ordered arrangement on the A and A′ sites, respectively, Fig. 6. The Ca^{2+} ions (green spheres) form a body centred arrangement in a double perovskite-type cubic cell in which the Cu^{2+} ions (yellow spheres) are located on the face and edge centres of the cell and form square-planar CuO_4 units. Despite its interesting crystal structure, there is no evidence for any structural phase transitions and CCTO remains cubic and centrosymmetric between ∼35 and 1000 K. There is an antiferromagnetic phase transition below 25 K but this temperature is well below that of major changes observed in the electrical properties.[50]

The electrical properties of CCTO started to attract attention around 20 years ago with reports of "giant" or "colossal" room temperature permittivity in CCTO single crystals,[51] thin films[52] and ceramics.[50] All measurements were based on fixed frequency, variable temperature permittivity and tan δ data in the Hz to MHz ranges and ∼10 to 400 K. An example dataset for a CCTO ceramic is shown in Fig. 6a for the effective permittivity of the sample, $\varepsilon_{eff} = C/\varepsilon_o$, where C is the measured capacitance at a specific (radio) frequency corrected for overall sample geometry, Eq. 7; tan δ is a geometry-independent parameter defined by the ratio $\varepsilon''/\varepsilon'$.

There were several unusual features associated with these DS results that were difficult to rationalise with the known crystallography of CCTO. First, the very large permittivity value, >7,000, across a wide temperature range, ∼100 to 400 K was unexpected for the centrosymmetric structure of CCTO in which there was no obvious source of dipole moment that could support such a high value permittivity. Second, a decrease in ε_{eff} by two orders of magnitude with decreasing temperature was observed that was strongly frequency- and temperature-dependent but attained a frequency independent value of ∼100 at ∼100 K with no evidence of any structural phase transition in this range. Third, a thermally activated peak in tan δ appeared to correlate with switching from $\varepsilon_{eff} \sim 100$ below 100 K to $\varepsilon_{eff} > 10{,}000$ at room temperature, (a). Fourth, the frequency, ω_o of the peak in tan δ occurred over a wide temperature range, (a). Fifth, ε_{eff} of single crystal CCTO[51] was at least one order of magnitude greater than that of ceramics[50] at room temperature which would not be expected if the time constants associated with DS data were linked to intrinsic behaviour, (b). Sixth, ε_{eff} at room temperature changed dramatically from ∼10,000 to >300,000 as the grain size in ceramic samples increased[53] and the magnitude of the tan δ peak and ω_o values for single crystal CCTO, (c), were substantially different from that of CCTO ceramics, (a); neither of these effects would be expected if the time constants associated with the DS data were linked to intrinsic behaviour.

These issues were resolved by adopting an IS approach to data collection and analysis and in particular, inspecting data in formalisms other than ε^*.[54–56] Z* plots for a CCTO single crystal and a ceramic (both with sputtered Au electrodes) are shown in Fig. 7. Both show a semi-circular arc at low frequencies with a non-zero intercept at high frequencies, insets (a) and (b). Measurements performed below ∼100 K showed the non-zero intercept developed into a high frequency Z* arc, (c) whereas the large low frequency arc was mainly out of the measurement range. On this basis, the IS data were modelled, to a first approximation, on two parallel RC elements, R_1C_1 and R_2C_2 connected in series, (d).

For both samples, R_1C_1 represents the high frequency data and corresponds to the semiconducting bulk response of CCTO. R_2C_2 represents an extrinsic contribution associated with a resistive grain boundary in the ceramic and a non-ohmic electrode

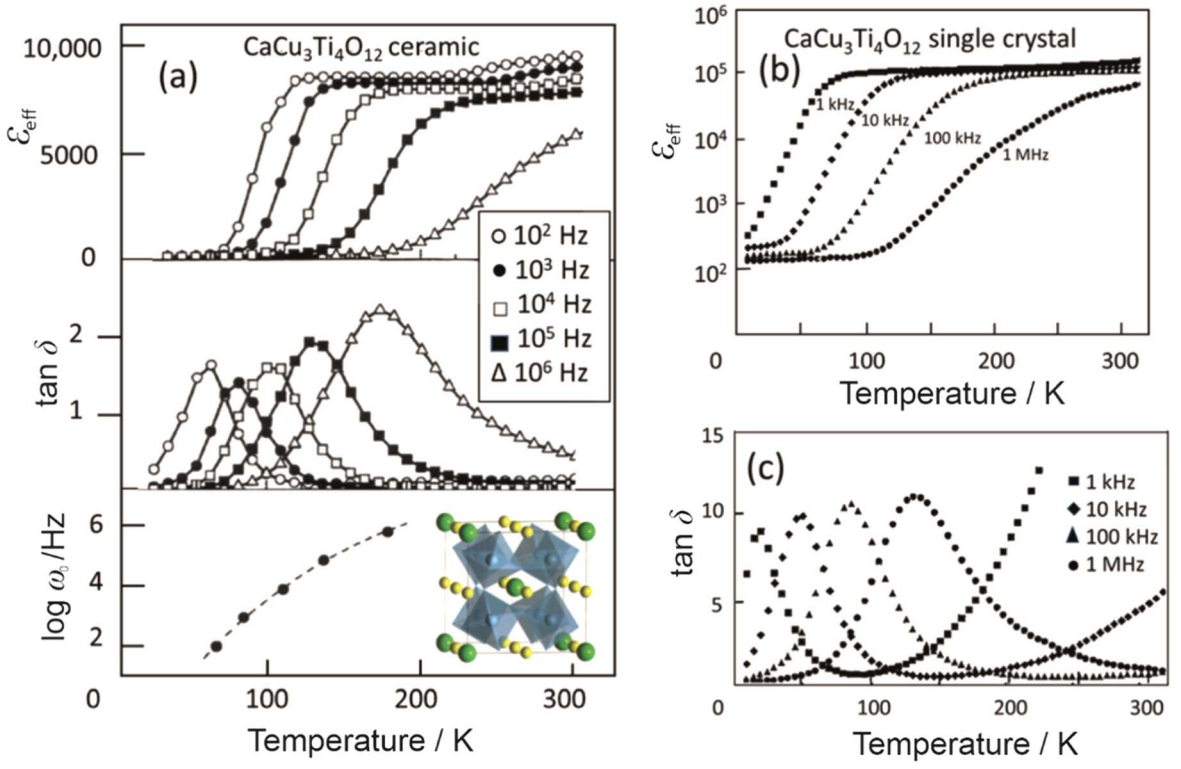

Figure 6. Dielectric data for (a) CCTO ceramics and (b, c) single crystals; (a) adapted from Ref. 50.

contact (Schottky barrier) in the single crystal. Reasoning is as follows:

At room temperature, the time constant, τ_1, of component R_1C_1 is small; from Eqs. 1, 2, $\omega_{max(1)}$ is outside the measuring frequency range and, other than a non-zero intercept in the Z* plot which represents R_1 (a,b), no information can be obtained about C_1. Assignment of an RC element to the bulk response is based on the magnitude of the capacitance which is why low temperature measurements (c) are required so that $\omega_{max(1)}$ occurs in the measured frequency range. From such high frequency arcs at low temperatures (c), C_1 was estimated using Eq. 2, converted to permittivities using Eqs. 7, 8) and shown as a function of temperature in Fig. 8a to reveal the true, temperature-dependent bulk permittivity of CCTO which is ~180 to 120 over the temperature range ~10 to 100 K for both single crystal and ceramics.

These permittivity values are in excellent agreement for the two samples and reveal a low temperature paraelectric response consistent with incipient ferroelectric behaviour (i.e. the permittivity increases with decreasing temperature, consistent with Curie-Weiss behaviour, but never reaches the ferroelectric state). Similar behaviour is observed for other tilted titanate perovskites such as $(Sr,Ca)TiO_3$.[57,58]

Conductivity data for R_1 are shown in Arrhenius format, (b) with activation energy ~80 meV, indicating a semiconducting bulk which supports the description of CCTO as a "leaky dielectric." The modest level of bulk semiconductivity can be suppressed by partial replacement of Cu with Mn on the A' sites to produce ceramics that are potentially useful as microwave dielectrics, with room temperature permittivity of ~93, a quality factor of ~3950 GHz (at 3.95 GHz) and a temperature coefficient of resonant frequency ~+657 ppm/K.[59]

The time constant, τ_2 for R_2C_2 occurs in the measured frequency range at room temperature where it dominates the measured electrical properties. Using data from the semicircle maxima in Z* plots in Fig. 7a, 7b), $C_2 \sim 10.7$ and ~0.6 nFcm^{-1} for the single crystal and ceramic, respectively. These values correspond to ε_{eff} of ~121 000 and ~6 800 and are the origin of the reported "giant" or "colossal permittivity" in the various forms of CCTO. The magnitude and temperature dependence of τ_2 ($=1/\omega_{max(2)}$) obtained from the low frequency arc in Z* for the two samples are significantly different, as shown in Fig. 8c, which is further proof of the different sources of τ_2. This also explains why ω_o values from the tan δ peaks in the DS data are different for CCTO crystals and ceramics, Figs. 6a, 6c.

The magnitude of C_2, and therefore ε_{eff}, is an order of magnitude larger for the single crystal ($\varepsilon_{eff} > 100\,000$) than the ceramic ($\varepsilon_{eff} \sim 7\,000$), consistent with most existing literature. The only reports for ceramics with $C_2 > 10$ nF cm^{-1} (and therefore $\varepsilon_{eff} > 100\,000$) are for large (100 to 300 μm) grain-sized ceramics.[53] The grain-size dependence of C_2 for CCTO ceramics has been well documented and is consistent with an Internal Barrier Layer Capacitance (IBLC) model as an explanation for the giant ε_{eff} observed for CCTO ceramics.[60,61] The activation energy for R_2 of ~0.6 eV in ceramics is consistent with the development of Schottky barriers at the grain boundaries, Fig. 8b.

The different origin of τ_2 in ceramic and single crystal samples was clarified and further emphasised by changing the electrodes from Au to InGa.[55] This had little effect on the ceramic impedance results (not shown), but had a dramatic effect on the low frequency arc for the single crystal, Fig. 8d. Using InGa electrodes, values were: $R_2 \sim 8\ \Omega$ cm; $C_2 \sim 21.6$ nF cm^{-1} ($\varepsilon_{eff} \sim 244\,000$); $R_1 \sim 14\ \Omega$ cm. For Au electrodes, $R_2 \sim 200\ \Omega$ cm and $R_1 \sim 14\ \Omega$ cm. It is well-recognised that changing the work function of a metal electrode used to contact a

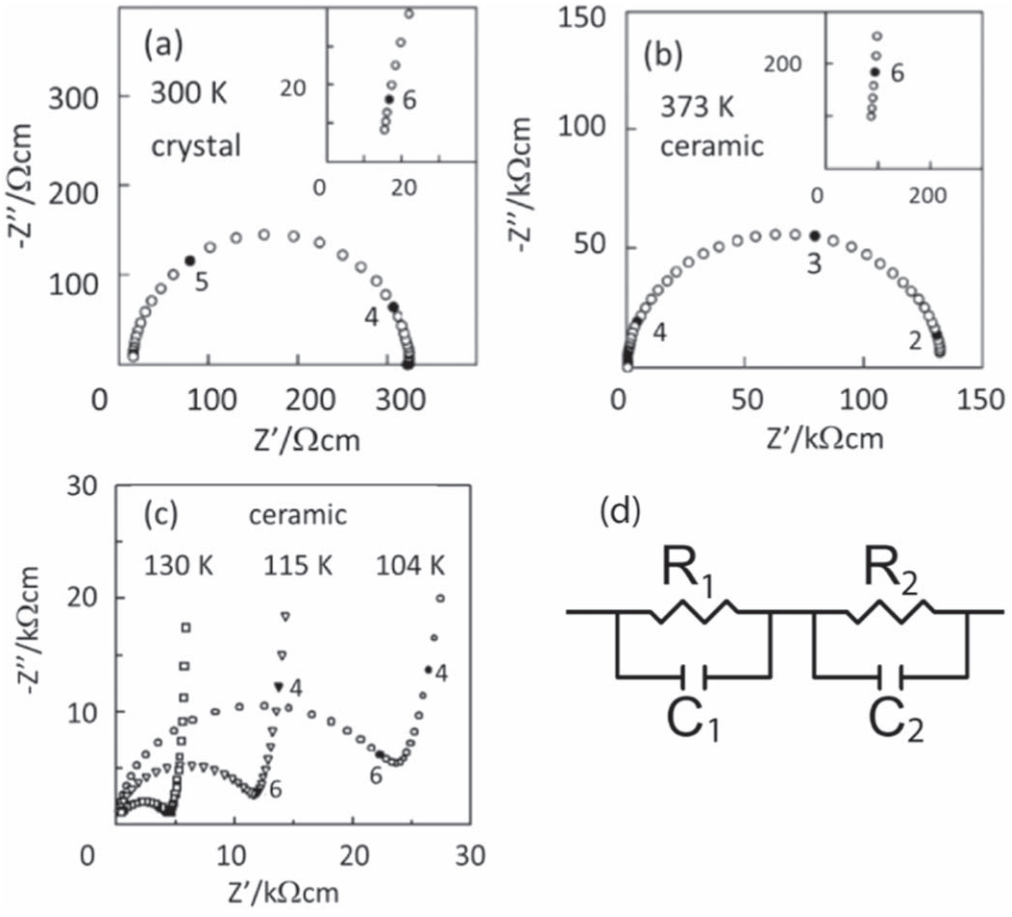

Figure 7. Impedance data for CCTO crystal and ceramic showing the effect of temperature. (a) and (b) adapted from Ref. 55 and (c) adapted from Ref. 54.

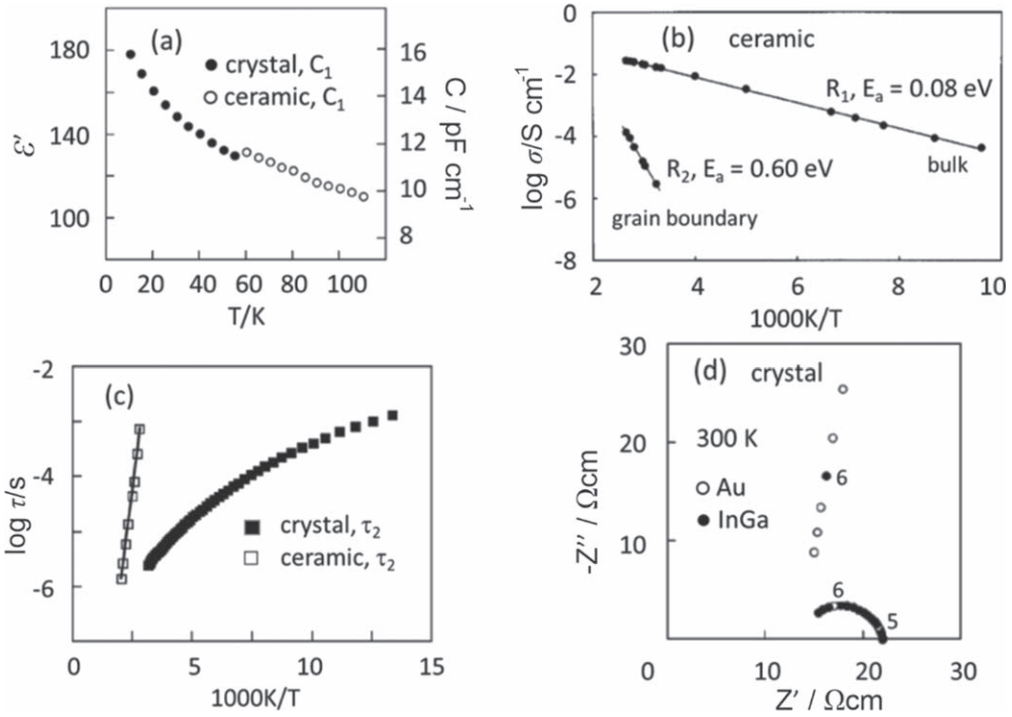

Figure 8. Comparisons of bulk and grain boundary/electrode contact impedances for CCTO ceramic and single crystal. (a), (c) and (d) adapted from Ref. 55 and (b) adapted from Ref. 54.

semiconducting material often produces different Schottky barrier heights and this is the source of the high ε_{eff} in CCTO crystals based on impedance measurements close to room temperature.

In conclusion, use of the terms "giant" and "colossal" for CCTO usually refers to the results of fixed frequency (but frequency-dependent) capacitance and permittivity measurements and not to the intrinsic ε_∞ bulk values which may be several orders of magnitude smaller. The capacitance C_2 values are several orders of magnitude higher than expected because they refer to thin regions, such as grain boundaries or electrode-sample contacts and because the experimental data have not been corrected for the actual geometry of these regions. Variable frequency IS data linked to equivalent circuit analysis is essential to analyse heterogeneous materials or devices such as this and to determine which time constants are represented in the various formalisms and methods of data presentation. Use of fixed frequency DS data is limited to studying the temperature dependence of certain time constants but without validation of the most appropriate equivalent circuit or the possible characterisation of departures from ideality represented by a CPE(s).

Case study 2: Lead Magnesium Niobate, PMN Relaxor Ferroelectric

High permittivity ceramics have been of much interest for many years; their permittivity is usually high over wide frequency and temperature ranges leading to numerous high permittivity applications. In many cases, temperature- and frequency-independence is achieved by the deliberate fabrication of materials that are compositionally heterogeneous, such as ceramics with a core–shell structure prepared by controlled in-diffusion of dopants. They are usually insulators, perhaps with a low level of leakage conductivity at higher temperatures.

Relaxors form a separate class of related, high permittivity, insulating materials. They are often compositionally homogeneous single crystals or ceramics and may be ferroelectric, but exhibit permittivity maxima that depend on both temperature and measuring frequency. Since their permittivity properties are of most interest, they are usually characterised by fixed frequency DS and, with their high *dc* resistances over the range of interest for potential applications, they have not been studied in much detail by broadband IS or DS.

Lead magnesium niobate, PMN, $Pb(Mg_{1/3}Nb_{2/3})O_3$, is the classic relaxor material with a record bulk permittivity of ~20,000.[62] It has a perovskite structure with Mg^{2+} and Nb^{5+} cations disordered over the octahedral B sites. The larger Mg^{2+} ion is perceived to occupy undistorted octahedral sites but the smaller Nb^{5+} ion causes distortion and polarity of its octahedral sites; in addition, local order within the random distribution of B site cations may lead to the formation of chemically ordered regions.[63] The Pb^{2+} cation is highly polarisable because it has two electrons located in non-bonding 6(s,p) hybridised orbitals; small, collective, off-centre displacements of Pb^{2+} ions from their A site location give rise to polar nano-regions and are currently regarded as the main source of polarity and high permittivity of PMN.[64–67]

PMN is commonly characterised using fixed frequency DS data, as shown for single crystal data in Fig. 9.[68] The real, ε' and imaginary, ε'' parts of the complex permittivity, ε^* both show broad maxima whose magnitudes and temperatures are frequency-dependent, as shown by the five datasets in (a). These data are typical of many literature reports of PMN and other relaxors. Given the limitations of fixed frequency DS, few attempts have been reported of data interpretation in terms of an equivalent circuit or the possible extraction of intrinsic electrical component values such as ρ and ε_∞.

PMN is a near-perfect insulator as shown in (b) by Z^* data at one temperature, 180 K, presented in the impedance complex plane. A spike is observed that passes through the origin at high frequencies and represents a capacitor in parallel with a resistor whose value was too large to measure. Much more information was obtained by converting the IS data to admittance and permittivity formalisms using Eqs. 10, 12, with results shown as spectroscopic plots of C′ and log Y′ in Fig. 10. C′ data, (a,b) show a dispersion over the four decades of measuring frequency and over the temperature range 180–260 K. The C′ data level off to constant values at lower frequencies and higher temperatures, (b,c). Y′ data show a power law response for temperatures up to 250 K (d), a more complex

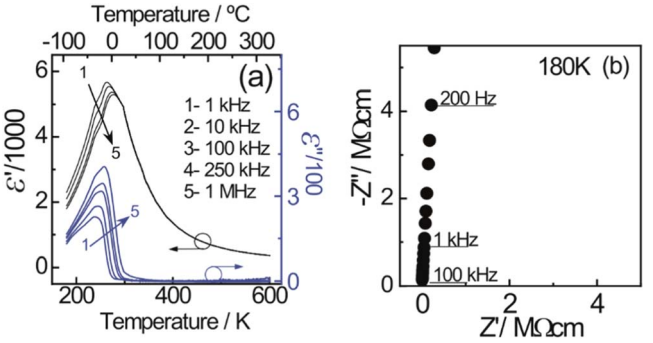

Figure 9. Permittivity and impedance data for PMN single crystal, adapted from Ref. 68.

response at higher temperatures (e) and completely insulating behaviour above 290 K as shown by an inability to obtain Y′ data at e.g. 300 K due to limitations of the measuring equipment.

Equivalent circuit analysis[68] showed that this entire C′, Y′ response, over the same temperature range, ∼180–290 K, that fixed frequency permittivity data showed relaxor behaviour, was dominated by the presence of a CPE in a simple series circuit element, Fig. 11a. An excellent fit between experimental and fitted data was obtained. At 300 K and above, the behaviour shown in Fig. 10c simplified to that of a perfect capacitor, Fig. 11b.

Fitted values of the circuit elements n_1, A_1, B_1 for CPE_1 and C_2, over the relaxor range 180–300 K, are shown in Fig. 12. The CPE n_1 value approaches unity at the lowest temperatures at which the CPE is almost entirely capacitive. Above ∼240 K, n starts to decrease rapidly as the conductive component, A_1 of the CPE becomes more important and probably reaches zero above about 290 K at which point the CPE is entirely conductive. The magnitude of A_1 increases by eight orders of magnitude over the relaxor temperature range and shows why CPE_1 becomes negligible as a series resistor above 290 K; the circuit therefore reduces to that of the capacitor C_2, Fig. 11b. At still higher temperatures, above about 600 K and well

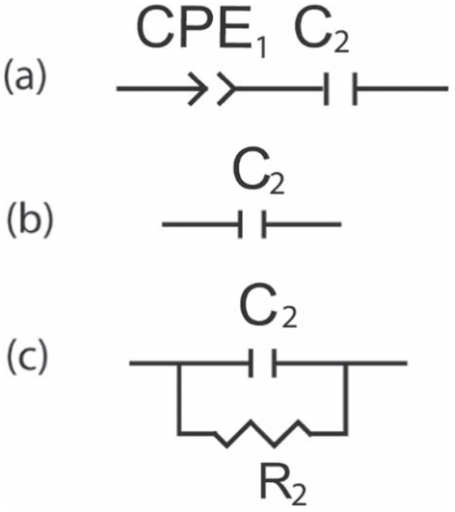

Figure 11. Equivalent circuits used to analyse and fit PMN impedance data.

beyond the conditions for relaxor behaviour, C_2 starts to act as a slightly leaky capacitor and the circuit acquires a finite resistance R_2 in parallel with C_2, Fig. 11c.

The realisation that a CPE is responsible for the permittivity dispersions shown in Fig. 9a and that, without a CPE, there would be no relaxor effect, gives new insight into relaxors.[68] It provides an entirely new methodology, based on IS and equivalent circuit modelling, for studying relaxors. The values and significance of the CPE parameters change greatly during the relaxor temperature range, Fig. 12 and therefore, a combination of broadband IS (or DS) data and equivalent circuit analysis are essential to obtain this information. In order for fixed frequency, variable temperature DS scans to provide the same information, it would be necessary that the measured permittivities were not frequency-dependent; clearly, this is not the case.

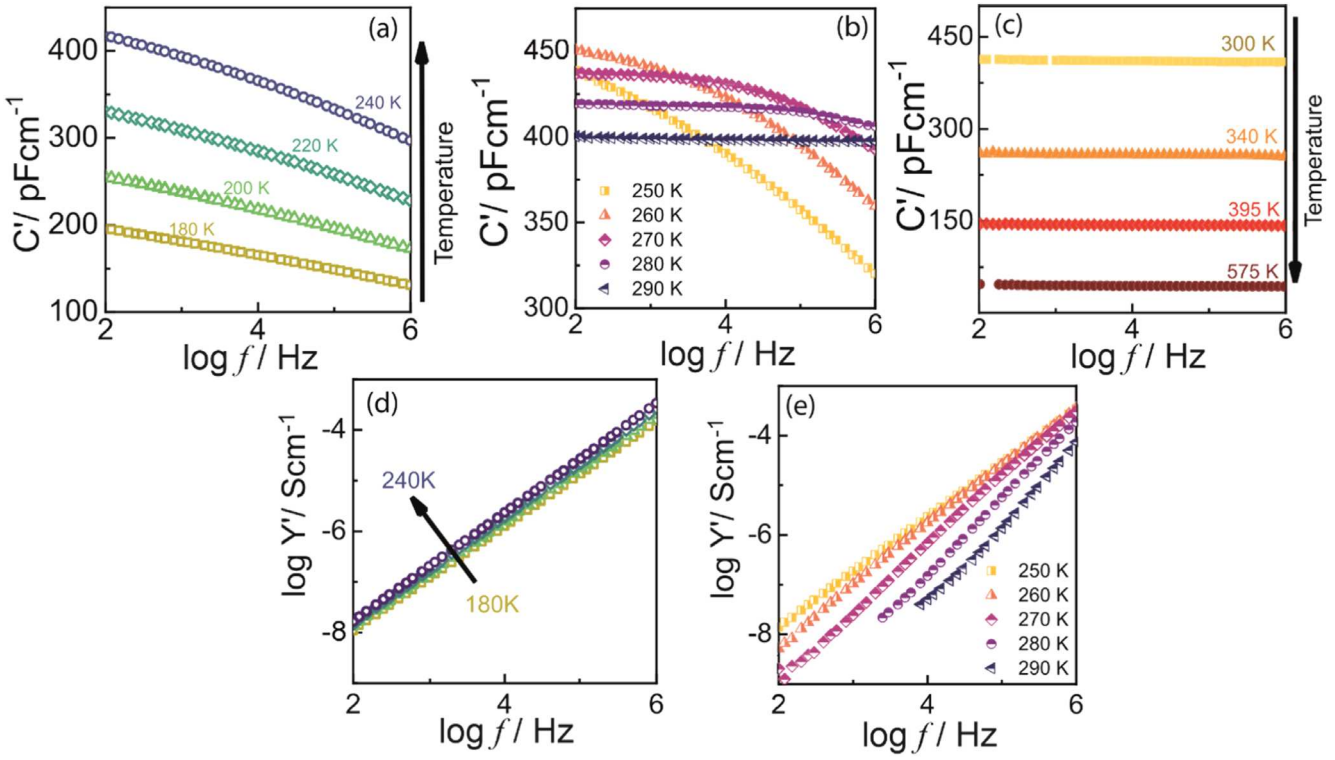

Figure 10. Frequency-dependent capacitance and admittance data at different temperatures for PMN crystal, adapted from Ref. 68.

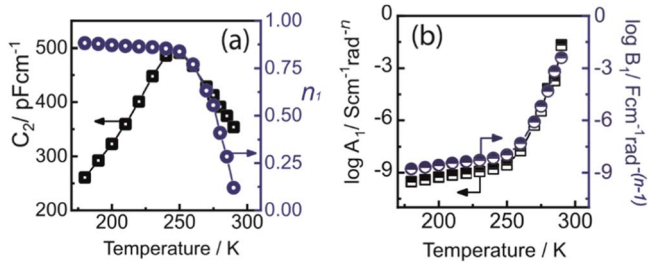

Figure 12. Temperature dependence over relaxor range of fitted parameter values using equivalent circuit, Fig. 11a, adapted from Ref. 68.

Conclusions

We have chosen two examples of different functional materials that require variable frequency impedance, or dielectric, data sets in order to separate their overall electrical properties into the contributing resistance and capacitance components. To quantify these components, it is essential to know the most appropriate equivalent circuit and therefore, the correct equations to use. Identification of the equivalent circuit enables assignment of the resistance and capacitance parameters to regions of the sample being measured.

Impedance or permittivity measurements of materials whose equivalent circuits consist of various R and C combinations in series and/or in parallel are always frequency-dependent. Fixed frequency measurements usually give mixed data that do not represent single components, leading to uncertainty over the significance of the data values and their interpretation. From fixed frequency data alone, it is not possible to determine which equivalent circuit represents a particular data set.

The electrical properties of most materials cannot be represented quantitatively by equivalent circuits that consist of ideal, frequency-independent resistors and capacitors. In earlier times, various distribution of relaxation time functions were used to characterise departures from ideality. As measurement techniques have advanced to permit broadband impedance and dielectric measurements, it has been realised, following the work of Jonscher and others, that non-ideality often takes the form of a power law frequency dependence. Data can now be analysed quantitatively in terms of constant phase elements which are parallel combinations of linked, frequency-dependent resistors and capacitors. These are characterised by an n parameter that determines the relative importance of resistive and capacitive contributions to a CPE and were shown by Almond and colleagues to depend directly on the number and nature of R, C links in complex equivalent circuits.

CPEs, and their n parameter, were often regarded merely as a "fudge factor" to obtain good fits of experimental data to equivalent circuits. The recognition that the electrical properties of relaxors such as PMN can be modelled entirely by the incorporation of a CPE into a simple series RC circuit shows that indeed, CPEs are more than just a fudge factor: without the non-ideality of circuits that can be modelled using CPEs, relaxors would not exist.

ORCID

Julia Ramírez-González https://orcid.org/0000-0002-6950-1255
Derek C. Sinclair https://orcid.org/0000-0002-8031-7678
Anthony R. West https://orcid.org/0000-0002-5492-2102

References

1. E. Barsoukov and J. R. Macdonald, *Impedance Spectroscopy: Theory, Experiment, and Applications* (John Wiley & Sons, NJ) 3rd ed. (2018).
2. V. V. Daniel, *Dielectric relaxation* (Academic, London and New York) (1967).
3. A. K. Jonscher, *Dielectric Relaxation in Solids* (Chelsea Dielectric Press, London) (1983).
4. S. Wang, J. Zhang, O. Gharbi, V. Vivier, M. Gao, and M. E. Orazem, "Electrochemical impedance spectroscopy." *Nature Reviews Methods Primers*, **1**, 41 (2021).
5. K. S. Cole and R. H. Cole, "Dispersion and absorption in dielectrics: I. Alternating current characteristics." *J. Chem. Phys.*, **9**, 341 (1941).
6. A. D. Franklin and H. J. De Bruin, "The fourier analysis of impedance spectra for electrode electrolytes." *Phys. Stat. Solidi*, **75**, 647 (1983).
7. A. K. Jonscher, "The "universal" dielectric response." *Nature*, **267**, 673 (1977).
8. E. J. Abram, D. C. Sinclair, and A. R. West, "A strategy for analysis and modelling of impedance spectroscopy data of electroceramics: doped lanthanum gallate." *J Electroceram*, **10**, 165 (2003).
9. J. E. Bauerle, "Study of solid electrolyte polarization by a complex admittance method." *J. Phys. Chem. Solids*, **30**, 2657 (1969).
10. J. T. S. Irvine, D. C. Sinclair, and A. R. West, "Electroceramics: characterization by impedance spectroscopy." *Adv Materials*, **2**, 132 (1990).
11. F. Kremer and A. Schönhals, *Broadband Dielectric Spectroscopy* (Springer, Berlin, Leipzig) (2003).
12. J. P. Runt and J. J. Fitzgerald, *Dielectric Spectroscopy of Polymeric Materials: Fundamentals and Applications* (American Chemical Society Books, Washington) (1997).
13. P. Lunkenheimer, M. Köhler, S. Kaster, and A. Loidl, "Dielectric spectroscopy of glassy dynamics." *Structural Glasses and Supercooled Liquids: Theory, Experiment, and Applications*, ed. P. G. Wolynes and V. Lubchenko (John Wiley & Sons) (2012).
14. J. Zhang, Y. Luo, Z. Yue, and L. Li, "Temperature stability, low loss and defect relaxation of MgO-TiO_2 microwave dielectric ceramics modified by $Ca_{0.8}Sr_{0.2}TiO_3$." *Ceram. Int.*, **44**, 141 (2018).
15. T. Fan, C. Ji, G. Chen, W. Cai, R. Gao, X. Deng, Z. Wang, and C. Fu, "Enhanced the dielectric relaxation characteristics of $BaTiO_3$ ceramic doped by $BiFeO_3$ and synthesized by the microwave sintering method." *Mater. Chem. Phys.*, **250**, 123034 (2020).
16. S. Siragam, R. S. Dubey, and L. Pappula, "Analysis of dielectric properties of zinc aluminum silicate based ceramic nanoparticles." *Mater. Today Proc.*, **45**, 2801 (2021).
17. B. Mohanty, S. Bhattacharjee, S. N. Sarangi, N. C. Nayak, R. K. Parida, and B. N. Parida, "Dielectric, electrical and magnetic characteristics of BST modified BLFO lead free ceramic." *J. Alloys Compd.*, **863**, 158060 (2021).
18. A. Orliukas, P. Bohac, K. Sasaki, and L. Gauckler, "Relaxation dispersion of ionic conductivity in a $Zr_{0.85}Ca_{0.15}O_{1.85}$ single crystal." *J. Eur. Ceram. Soc.*, **12**, 87 (1993).
19. M. A. Subramanian, L. Dong, N. Duan, B. A. Reisner, and A. W. Sleight, "High dielectric constant in $ACu_3Ti_4O_{12}$ and $ACu_3Ti_3FeO_{12}$ phases." *J. Solid State Chem.*, **151**, 323 (2000).
20. P. Jha, S. Rai, K. V. Ramanujachary, S. E. Lofland, and A. K. Ganguli, "$La_{0.4}Ba_{0.4}Ca_{0.2})(Mn_{0.4}Ti_{0.6})O_3$: a new titano-manganate with a high dielectric constant and antiferromagnetic interactions." *J. Solid State Chem.*, **177**, 2881 (2004).
21. P. Lunkenheimer, S. Krohns, S. Riegg, S. G. Ebbinghaus, A. Reller, and A. Loidl, "Colossal dielectric constants in transition-metal oxides." *Eur. Phys. J. Special Topics*, **180**, 61 (2010).
22. W. Hu et al., "Electron-pinned defect-dipoles for high performance colossal permittivity materials." *Nat. Mater.*, **12**, 821 (2013).
23. W. Dong, W. Hu, A. Berlie, K. Lau, H. Chen, R. L. Withers, and Y. Liu, "Colossal dielectric behavior of Ga+Nb co-doped rutile TiO_2." *ACS Appl. Mater. Interfaces*, **7**, 25321 (2015).
24. H. Taniguchi, D. Sato, A. Nakano, and I. Terasaki, "Permittivity boosting in "yellow" (Nb + In) co-doped TiO_2." *J Mat Chem C*, **8**, 13627 (2020).
25. S. Kakimoto, Y. Hashimoto, T. Kuwano, K. Kimura, K. Hayashi, M. Hagiwara, K. Deguchi, and H. Taniguchi, "Controlling dielectric properties of Nb + X (X = Al, Ga, In) co-doped and Nb-doped rutile-type TiO_2 single crystals." *J Mat. Chem. C*, **11**, 1304 (2023).
26. P. G. Bruce and A. R. West, "The ac conductivity of polycrystalline LISICON, Li_{2+2x} Zn_{1-x} GeO_4, and a model for intergranular constriction resistances." *J. Electrochem. Soc.*, **130**, 662 (1983).
27. J. L. Pautrat, B. Katircioglu, N. Magnea, D. Bensahel, J. C. Pfister, and L. Revoil, "Admittance spectroscopy: a powerful characterization technique for semiconductor crystals—application to ZnTe." *Solid. State. Electron.*, **23**, 1159 (1980).
28. T. P. Weiss, S. Nishiwaki, B. Bissig, S. Buecheler, and A. N. Tiwari, "Voltage dependent admittance spectroscopy for the detection of near interface defect states for thin film solar cells." *Phys. Chem. Chem. Phys.*, **19**, 30410 (2017).
29. J. Bollmann and A. Venter, "Admittance spectroscopy or deep level transient spectroscopy: a contrasting juxtaposition." *Phys. B Condens. Matter*, **535**, 237 (2018).
30. J. V. Li, "Defect characterization using raw admittance spectroscopy." *J. Phys. Chem. C*, **125**, 2860 (2021).
31. I. M. Hodge, M. D. Ingram, and A. R. West, "Impedance and modulus spectroscopy of polycrystalline solid electrolytes." *J. Electroanal. Chem. Interfacial Electrochem.*, **74**, 125 (1976).
32. D. P. Almond and A. R. West, "Impedance and modulus spectroscopy of "real" dispersive conductors." *Solid State Ionics*, **11**, 57 (1983).
33. D. C. Sinclair and A. R. West, "Impedance and modulus spectroscopy of semiconducting $BaTiO_3$ showing positive temperature coefficient of resistance." *J. Appl. Phys.*, **66**, 3850 (1989).
34. D. C. Sinclair, "Characterization of electro-materials using ac impedance spectroscopy." *Bol Soc Espanola de Ceramica y Vidrio*, **65**, 55 (1995).
35. C. T. Moynihan, "Analysis of electrical relaxation in glasses and melts with large concentrations of mobile ions." *J Non Cryst Solids*, PART 2 **172–174**, 1395 (1994).
36. D. W. Davidson and R. H. Cole, "Dielectric relaxation in glycerine." *J. Chem. Phys.*, **18**, 1417 (1950).

37. S. Havriliak and S. Negami, "A complex plane representation of dielectric and mechanical relaxation processes in some polymers." *Polymer (Guildf)*, **8**, 161 (1967).
38. A. K. Jonscher, R. Holloway, and B. N. College, "The "universal" dielectric response: Part I." *IEEE Electr. Insul. Mag.*, **6**, 19 (1990).
39. A. K. Jonscher, "The "universal" dielectric response: Part II." *IEEE Electr. Insul. Mag.*, **6**, 24 (1990).
40. A. K. Jonscher, "The "universal" dielectric reponse: Part III." *IEEE Electr. Insul. Mag.*, **6**, 19 (1990).
41. R. J. Grant, I. M. Hodge, M. D. Ingram, and A. R. West, "Conductivity dispersion in single crystal β-alumina electrolyte." *Nature*, **266**, 42 (1977).
42. D. Perry and M. Mamlouk, "Probing mass transport processes in Li-ion batteries using electrochemical impedance spectroscopy." *J. Power Sources*, **514**, 230577 (2021).
43. P. Zoltowski, "On the electrical capacitance of interfaces exhibiting constant phase element behaviour." *J. Electroanal. Chem.*, **443**, 149 (1998).
44. J. Bisquert, G. Garcia-Belmonte, P. Bueno, E. Longo, and L. O. S. Bulhões, "Impedance of constant phase element (CPE)-blocked diffusion in film electrodes." *J. Electroanal. Chem.*, **452**, 229 (1998).
45. D. P. Almond and C. R. Bowen, "Anomalous power law dispersions in ac conductivity and permittivity shown to be characteristics of microstructural electrical networks." *Phys. Rev. Lett.*, **92**, 1 (2004).
46. D. P. Almond, C. R. Bowen, and D. A. S. Rees, "Composite dielectrics and conductors: simulation, characterization and design." *J. Phys. D: Appl. Phys.*, **39**, 1295 (2006).
47. C. R. Bowen and D. P. Almond, "Modelling the "universal" dielectric response in heterogeneous materials using microstructural electrical networks." *Mat Sci Tech*, **22**, 719 (2006).
48. D. P. Almond and B. Vainas, "The dielectric properties of random R-C networks as an explanation of the "universal" power law dielectric response of solids." *J Phys Cond Matter*, **11**, 9081 (1999).
49. B. Vainas, D. P. Almond, J. Luo, and R. Stevens, "An evaluation of random R-C networks for modelling the bulk ac electrical response of ionic conductors." *Solid State Ionics*, **126**, 65 (1999).
50. A. P. Ramirez, M. A. Subramanian, M. Gardel, G. Blumberg, D. Li, T. Vogt, and S. M. Shapiro, "Giant dielectric constant response in a copper-titanate." *Solid State Commun.*, **115**, 217 (2000).
51. C. C. Homes, T. Vogt, S. M. Shapiro, S. Wakimoto, and A. P. Ramirez, "Optical response of high-dielectric-constant perovskite-related oxide." *Science*, **293**, 673 (2001).
52. G. Deng, Z. He, and P. Muralt, "Physical aspects of colossal dielectric constant material $CaCu_3Ti_4O_{12}$ thin films." *J. Appl. Phys.*, **105**, 084106 (2009).
53. T. B. Adams, D. C. Sinclair, and A. R. West, "Giant barrier layer capacitance effects in $CaCu_3Ti_4O_{12}$ ceramics." *Adv. Mater.*, **14**, 1321 (2002).
54. D. C. Sinclair, T. B. Adams, F. D. Morrison, and A. R. West, "$CaCu_3Ti_4O_{12}$: a one-step internal barrier layer capacitor." *Appl. Phys. Lett.*, **80**, 2153 (2002).
55. M. C. Ferrarelli, D. C. Sinclair, A. R. West, H. A. Dabkowska, A. Dabkowski, and G. M. Luke, "Comment on the origin(s) of the giant permittivity effect in $CaCu_3Ti_4O_{12}$ single crystals and ceramics." *J Mat Chem*, **19**, 5916 (2009).
56. M. Li, A. Feteira, D. C. Sinclair, A. R. West, Z. Shen, and M. Nygren, "Origin(s) of the apparent high permittivity in $CaCu_3Ti_4O_{12}$ ceramics: clarification on the contributions from internal barrier layer capacitor and sample: electrode contact effects." *J. Appl. Phys.*, **106**, 104106 (2009).
57. K. A. Müller and H. Burkard, "$SrTiO_3$: an intrinsic quantum paraelectric below 4 K." *Phys. Rev. B*, **19**, 3593 (1979).
58. V. V. Lemanov, A. V. Sotnikov, E. P. Smirnova, M. Weihnacht, and R. Kunze, "Perovskite $CaTiO_3$ as an incipient ferroelectric." *Solid State Commun.*, **110**, 611 (1999).
59. M. Li, A. Feteira, D. C. Sinclair, and A. R. West, "Dielectric and microwave dielectric resonance properties of $CaCu_{2.85}$ $Mn_{0.15}Ti_4O_{12}$ ceramics." *Appl. Phys. Lett.*, **91**, 13291 (2007).
60. T. B. Adams, D. C. Sinclair, and A. R. West, "Characterisation of grain boundary Impedances in fine and coarse grained $CaCu_3Ti_4O_{12}$ ceramics." *Phys. Rev. B*, **73**, 094124 (2006).
61. T. B. Adams, D. C. Sinclair, and A. R. West, "The influence of processing on the electrical properties of $CaCu_3Ti_4O_{12}$ ceramics." *J Amer. Ceram. Soc.*, **89**, 3129 (2006).
62. R. A. Cowley, S. N. Gvasaliya, S. N. Lushnikov, S. G. Roessli, and G. M. Rotaru, "Relaxing with relaxors: a review of relaxor ferroelectrics." *Adv. Phys.*, **60**, 229 (2011).
63. L. E. Cross, "Relaxor ferroelectrics." *Ferroelectrics*, **76**, 241 (1987).
64. T. Egami, "Microscopic model of relaxor phenomena in Pb-containing mixed oxides." *Ferroelectrics*, **222**, 163 (1999).
65. M. J. Cabral, S. Zhang, E. C. Dickey, and J. M. Lebeau, "Gradient chemical order in the relaxor PMN." *Appl. Phys. Lett.*, **112**, 082901 (2018).
66. M. Eremenko, V. Krayzman, A. Bosak, H. Y. Playford, K. W. Chapman, J. C. Woicik, B. Ravel, and I. Levin, "Local atomic order and hierarchical polar nanoregions in a classical relaxor ferroelectric." *Nat. Commun.*, **10**, 2728 (2019).
67. M. J. Krogstad et al., "The relation of local order to material properties in relaxor ferroelectrics." *Nat. Mater.*, **17**, 718 (2018).
68. X. Vendrell, J. Ramirez-Gonzalez, Z.-G. Ye, and A. R. West, "Revealing the role of the constant phase element in relaxor ferroelectrics." *Commun. Phys.*, **5**, 1 (2022).